Improved electrical mobility in highly epitaxial La:$BaSnO_3$ films on $SmScO_3$(110) substrates.

P.V. Wadekar[1], J. Alaria[2], M. O'Sullivan[1], N.L.O. Flack[1], T.D. Manning[1], L.J. Phillips[2], K. Durose[2], O.Lozano[3], S.Lucas[3], J. B. Claridge[1], M.J.Rosseinsky[1].

[1] *Department of Chemistry, University of Liverpool, Crown Street, Liverpool L69 7ZE, UK.*

[2] *Stephenson Institute for Renewable Energy & Department of Physics, University of Liverpool, Crown Street, Liverpool L69 7ZD, UK.*

[3] *Research Centre for the Physics of Matter and Radiation, Namur Research Institute for Life Sciences, University of Namur, Namur 500, Belgium.*

Heteroepitaxial growth of $BaSnO_3$ (BSO) and $Ba_{1-x}La_xSnO_3$ (x = 7%) (LBSO) thin films on different perovskite single crystal ($SrTiO_3$ (001) and $SmScO_3$ (110)) substrates has been achieved by Pulsed Laser Deposition (PLD) under optimized deposition conditions. X-ray diffraction measurements indicate that the films on either of these substrates are relaxed due to the large mismatch and present a high degree of crystallinity with narrow rocking curves and smooth surface morphology while analytical quantification by proton induced X-ray emission (PIXE) confirms the stoichiometric La transfer from a polyphasic target, producing films with measured La contents above the bulk solubility limit. The films show degenerate semiconducting behavior on both substrates, with the observed room temperature resistivities, Hall mobilities and carrier concentrations of 4.4 mΩcm, 10.11 $cm^2V^{-1}s^{-1}$, and 1.38×10^{20} cm^{-3} on $SmScO_3$ and 7.8 mΩcm, 5.8 $cm^2V^{-1}s^{-1}$, and 1.36×10^{20} cm^{-3} on $SrTiO_3$ ruling out any extrinsic contribution from the substrate. The superior electrical properties observed on the $SmScO_3$ substrate are attributed to reduction in dislocation density from the lower lattice mismatch.

Tin doped indium oxide (ITO, $In_{1.95}Sn_{0.05}O_3$) has been extensively studied as a transparent conducting oxide (TCO) because of the unusual combination of high transparency in the visible range coupled with metal-like resistivity (~10^{-1} mΩcm) and high mobility (10-200 $cm^2V^{-1}s^{-1}$ depending on the growth method). These properties make ITO important for optoelectronic devices such as flat panel displays, light emitting diodes and solar cells.[1] The high dispersion of the bottom of the *s*-type conduction band along with the lowered optical absorption due to hybridization between Sn and In *s* states produce the enhanced electrical and optical properties of ITO.[2]

However, the scarcity of indium had led to the search for other doped oxide semiconductors such as ZnO,[3] TiO_2[4] and SnO_2[5,6] that can be used as alternatives to ITO with resistivities approaching the application threshold of 10^{-1} mΩcm,[7] however device patterning and environmental stability issues are unresolved.[8,9] The rapid development of perovskite-based photovoltaic cells calls for compatible transparent electrodes.[10] Titanate-based perovskites have been heavily studied as potential TCOs,[11-13] and recently $BaSnO_3$ (BSO) has been proposed as a high mobility TCO because its conduction band is composed of Sn 5*s* orbitals and La doping will create free carriers.[14] Initial work on thin films of doped stannates indicated that while oriented growth is possible, the resistivities are one order of magnitude higher[15-19] than found for ITO. Subsequent work on lanthanum doped barium stannate (LBSO) epitaxial thin films on $SrTiO_3$ (001)[20,21] substrates challenged this picture with room temperature mobility (resistivity) of ~ 70 $cm^2V^{-1}s^{-1}$, (0.17 mΩcm), which are comparable to conventional ITO thin films.

In PLD stoichiometric transfer from the target is often assumed to be achieved, as done in previous work on LBSO films, but the analytical quantification of dopants which is crucial information in order to control and understand the electrical properties was not reported until

now, so determining the chemical and electrical properties is a priority. The high mobility compared to the previous results is attributed to a superior crystalline quality of these thin films[21] however; several other factors could be the origin of such results. Recent theoretical results highlight the possibility of tuning the bandgap using elastic strain, [22] and the interpretation of the electrical properties of films needs to take into account the role of any free carriers generated in the substrates during film deposition. Oxygen vacancies generated during growth at high temperatures and low pressures in $SrTiO_3$ can induce conductivity.[23, 24] All of these potential problems make it difficult to robustly separate the films electrical properties from those of the substrate. Moreover, it has been suggested that the observed mobility in the thin films could be improved by reducing the lattice mismatch between LBSO and the substrate.[20] In order to investigate these effects we have grown high quality BSO and LBSO films of experimentally determined composition on $SrTiO_3$ (001) (STO) [lattice mismatch of +5.28%] and $SmScO_3$ (110) (SSO) substrates [+3.08% lattice mismatch]. The scandate substrate possesses not only the largest lattice parameter of commercially available perovskite substrates, but is also redox-resistant to the introduction of carriers during processing, allowing for the investigation of possible strain effects and separation of the intrinsic electrical properties of the films.

Bulk targets of BSO and LBSO were prepared using $BaCO_3$, La_2O_3, and SnO_2 starting materials. Stoichiometric mixtures were ground, pressed and sintered at 1250 ^oC for 24 hours in alumina crucibles followed by grinding, after which the powders were isostatically pressed and fired at 1450 ^oC for 24 hours. XRD measurements showed that the cubic perovskite phase with space group $Pm\bar{3}m$ was formed in the undoped BSO targets. However in case of LBSO, since the solid solubility of lanthanum is 3%[25], a polyphasic target with both perovskite $Ba_{1-x}La_xSnO_3$ and pyrochlore phase $La_2Sn_2O_7$ was formed with weight fractions of 95.7(3) and 4.3(2)%

respectively. Epitaxial thin films of BSO and LBSO were grown on STO and SSO substrates using PLD with a 248 nm KrF laser. The vacuum chamber was pumped to a base pressure of 5×10^{-7} Torr. Prior to deposition 100 mTorr of O_2 gas was introduced in the chamber and substrates were annealed for 30 minutes. For all the depositions the laser energy was maintained at 180 mJ and frequency of 5 Hz. The numbers of pulses were adjusted to grow approximately 40 nm thick films. After growth, the samples were annealed for 10 minutes in 100 mTorr of O_2 gas and then cooled down to room temperature in the same oxygen pressure. Optimum growth was achieved for oxygen partial pressures of 2 mTorr and a heater temperature of 850 ^{o}C.

$\theta/2\theta$ scans were measured using a two circle Panalytical X'Pert PRO diffractometer (Co $K_{\alpha 1}$), while rocking curves (RC), X-ray reflectivity (XRR) and reciprocal space maps (RSMs) were measured using a four circle Panalytical X'Pert PRO diffractometer (Cu $K_{\alpha 1}$). Surface morphology was studied using an Agilent 5600LS atomic force microscope (AFM). The temperature dependent electrical properties (resistivity, carrier concentration) were measured using van der Pauw geometry in a commercial Semimetrics 4C system using gold contacts. Rutherford back scattering (RBS) and proton induced X-ray emission (PIXE) measurements were performed using a HVE Tandetron accelerator on thicker LBSO films grown under the same conditions as the film presented in this study in order to increase the volume probed. For RBS, a passive implanted planar silicon (PIPS) detector (Canberra) was used, while for PIXE, a low energy germanium (LEGe) detector (Canberra) was used. Protons of 2.5 MeV were used to bombard the samples positioned at 45°. Lanthanum quantification was performed in the L-shell energy window of 5.33-5.78 keV as the emission intensities are stronger. PIXE spectra were analyzed by the software GUPIXWIN, while RBS where analyzed by SimNRA.[26]

Figure 1 (a) and (c) show the wide range XRD θ-2θ scans for the BSO/STO and LBSO/STO, BSO/SSO and LBSO/SSO films respectively. On either of these substrates, the (00*l*) reflections from the film are observed, indicating oriented growth along the *c*-axis. No secondary phases have been observed. The bulk lattice constant of $BaSnO_3$ is 4.115(1) Å, while the measured out-of-plane lattice constant of BSO films on SSO and STO respectively are 4.117(2) Å and 4.122(1) Å, indicating that the undoped films are not completely relaxed. In the case of single phase bulk lanthanum doped $BaSnO_3$, the lattice constant increases by 0.072% to 4.118(4) Å for $Ba_{0.97}La_{0.03}SnO_3$ (x = 3%).[25] A similar trend is also observed in the La-doped thin films where the lattice constant increases to 4.122(1) Å and 4.127(1) Å on SSO and STO respectively, an expansion of 0.12% compared to the undoped films. Assuming the films follow the same Vegard's law variation observed in the bulk, this lattice expansion would correspond to a doping level of x = 5% in the films.

The crystalline quality is assessed by measuring the RC of the (002) reflection for the doped samples. The top left inserts in figures 1(a) and 1(c) show the fitted RC with full width half maximum (FWHM) values of 0.093^o and 0.090^o for LBSO/STO and LBSO/SSO respectively, comparable to the films of similar nominal compositions[20]. The Pendellosung fringes (middle inserts figure 1(a) and (c)) of the (002) Bragg peak of the films indicate that coherent growth with good crystallinity and smooth surfaces is sustained in the out-of-plane direction. Analysis of the Pendellosung fringes gives film thicknesses of 37.1 nm on STO and 34.7 nm on SSO substrates. AFM measurements showed that films on either substrate were smooth with a root mean square roughness of less than 0.6 nm and are in agreement with the XRR model.[27] Asymmetrical RSMs were measured to ascertain the strain state in these films (Figure 1(b) and (d) for STO and SSO respectively). LBSO films on either of the substrates are

not fully strained to the substrate due to the large mismatch, excluding the possibility of strain affecting the electrical properties. The more pronounced broadening in Q_x for the film grown on STO compared to the film grown on SSO indicates the presence of a larger number of dislocations in the film.

RBS was used to determine the film thickness, while PIXE was used for chemical quantification, with the results presented in figure 2(a) and 2(b) respectively. The film thickness was determined to be about 320 nm by simulating the RBS spectrum. PIXE data was analyzed using a variable width digital top hat filter function to suppress the background components and fitted using a least squares procedure. The atomic concentration of La was derived from the mass concentration data as follows: La and Ba unnormalized atomic concentrations were calculated as: $[X]_{at.\ conc.} = [Sn]_{at.\ conc.} * ([X]_{mass} / [Sn]_{mass}) * ([Sn]_{at.\ weight} / [X]_{at.\ weight})$, with [X]= La or Ba and $[Sn]_{at.\ conc.} = 1$, followed by a normalization using the sum of each atomic concentration. The La content was 8 ± 2% indicating that the targeted La doping level is achieved in the films, consistent with stabilization as films of compositions inaccessible in conventional bulk synthesis. If each La^{3+} dopant produces one free electron, the expected carrier concentration in the $Ba_{0.93}La_{0.07}SnO_3$ film would be 9.8×10^{20} cm^{-3}.

The electrical transport parameters (resistivity, carrier concentration and mobility) of the doped films are shown in figure 3(a) and 3(b) for LBSO/SSO and LBSO/STO respectively. Hall effect measurements showed that the majority carriers in the films are electrons and have a room temperature effective carrier concentration of 1.38×10^{20} cm^{-3} for LBSO/SSO and 1.36×10^{20} cm^{-3} for LBSO/STO, indicating that the number of free carriers donated by La is the same irrespective of the substrates on which the films are grown. Our measured carrier concentration values are also lower than expected assuming 1 electron/La and give a dopant activation rate of

14%. The analytically determined lanthanum doping in the present films is beyond the bulk solid solution limit and may drive enhanced carrier trapping associated with dopant clustering, producing the observed lower effective carrier concentrations,[29] which is different from other reports as no total dopant concentrations are analytically determined in those works [15,20,28]. The carrier concentration of films with similar targeted compositions varies from 2×10^{21} cm^{-3} (200 % dopant activation rate) to 7×10^{20} cm^{-3} (70 % dopant activation rate) [15,20] and the low activation rate observed in our films is not isolated in this system as a similar dopant activation rate was reported for a lower nominal La concentration of x = 0.04.[28] The temperature dependence is consistent with a mobility-controlled degenerate semiconductor in both cases, the resistivity being almost constant in the temperature range studied, as opposed to a conventional activated semiconductor where the resistivity decreases exponentially as the temperature increases. This metallic behavior is confirmed by the carrier concentration being independent of the temperature, only decreasing at low temperature when ionized dopants start to freeze-out. As a result, mobilities increase as the temperature is decreased and saturate near 40 K, suggesting that phonon scattering is the main process in this temperature regime. The films are more conducting on SSO than on STO (4.4 mΩcm and 7.8 mΩcm at room temperature respectively). Although similar FWHM are measured for the two films, dislocations that are formed due to lattice mismatch between film and substrate can reduce the mobility because they act as double Schottky barriers.[30] A slight improvement in the lattice mismatch reduces the scattering by dislocations thereby increasing the mobility, as seen for the films on STO (5.8 cm^2 $V^{-1}s^{-1}$ at room temperature) versus those on SSO (10.11 cm^2 $V^{-1}s^{-1}$ at room temperature). The mobilities obtained are consistent with the values expected for the total amount of impurity introduced in the lattice.[31]

In summary, we have grown heteroepitaxial thin films of BSO and LBSO on STO and SSO substrates by PLD. Analytical chemical quantification by PIXE measurements indicates that the lanthanum doping concentration is 8 ± 2% demonstrating that PLD gives higher La concentrations than possible in bulk ceramic synthesis. The influence of the substrate, specifically the lattice mismatch has been studied and we have shown that increased mobility can be achieved by lowering the misfit. The resulting compositionally characterised materials have electrical properties that are consistent across substrates with different mismatch and redox characteristics. The non-reproducibility of carrier concentration and mobility in this system reported in the literature for the same dopant concentration[15,20,28] highlight the need for a better understanding of the transport mechanism in this system. Increasing the carrier concentration to its nominal value without degrading the mobility would result in a conductivity of ~ 10^{-1} mΩcm which would provide an alternative indium free TCO.

This work is funded by the European Research Council (ERC Grant agreement 227987 RLUCIM).

References

[1]I. Hamberg and C. G. Granqvist, J. Appl. Phys. **60**, R123 (1986).

[2]O. N. Mryasov and A. J. Freeman, Phys. Rev. B **64**, 233111 (2001).

[3]E. M. Kaidashev, M. Lorenz, H. von Wenckstern, A. Rahm, H. C. Semmelhack, K. H. Han, G. Benndorf, C. Bundesmann, H. Hochmuth, and M. Grundmann, Appl. Phys. Lett. **82**, 3901 (2003).

[4]Y. Furubayashi, T. Hitosugi, Y. Yamamoto, K. Inaba, G. Kinoda, Y. Hirose, T. Shimada, and T. Hasegawa, Appl. Phys. Lett. **86**, 252101 (2005).

[5]H. Kim and A. Pique, Appl. Phys. Lett. **84**, 218 (2004).

[6]H. Toyosaki, M. Kawasaki, and Y. Tokura, Appl. Phys. Lett. **93**, 132109 (2008).

[7]K. Ellmer, Nat. Photonics **6**, 808 (2012).

[8]T. Minami and T. Miyata, Thin Solid Films **517**, 1474 (2008).

[9]T. Minami, Thin Solid Films **516**, 5822 (2008).

[10]I. Chung, B. Lee, J. He, R. P. Chang, and M. G. Kanatzidis, Nature **485**, 486 (2012).

[11]A. Biswas, N. Li, M. H. Jung, Y. W. Lee, J. S. Kim, and Y. H. Jeong, J. Appl. Phys. **113**, 183117 (2013).

[12]H. H. Wang, D. F. Cui, S. Y. Dai, H. B. Lu, Y. L. Zhou, Z. H. Chen, and G. Z. Yang, J. Appl. Phys. **90**, 4664 (2001).

[13]T. Zhao, H. B. Lu, F. Chen, S. Y. Dai, G. Z. Yang, and Z. H. Chen, J. Cryst. Growth **212**, 451 (2000).

[14]H. Mizoguchi, H. W. Eng, and P. M. Woodward, Inorg. Chem. **43**, 1667 (2004).

[15]H. F. Wang, Q. Z. Liu, F. Chen, G. Y. Gao, W. B. Wu, and X. H. Chen, J. Appl. Phys. **101**, 106105 (2007).

[16]Q. Z. Liu, H. F. Wang, F. Chen, and W. Wu, J. Appl. Phys. **103**, 093709 (2008).

[17]Q. Liu, J. Dai, Z. Liu, X. Zhang, G. Zhu, and G. Ding, J. Phys. D: Appl. Phys. **43**, 455401 (2010).

[18]H. Wang, X. Jiao, Q. Liu, X. Xuan, F. Chen, and W. Wu, J. Phys. D: Appl. Phys. **43**, 035403 (2010).

[19]Q. Z. Liu, J. M. Dai, X. B. Zhang, G. P. Zhu, Z. L. Liu, and G. H. Ding, Thin Solid Films **519**, 6059 (2011).

[20]H. J. Kim, U. Kim, T. H. Kim, J. Kim, H. M. Kim, B.-G. Jeon, W.-J. Lee, H. S. Mun, K. T. Hong, J. Yu, K. Char, and K. H. Kim, Phys. Rev. B **86**, 165205 (2012).

[21]H. Mun, U. Kim, H. M. Kim, C. Park, T. H. Kim, H. J. Kim, K. H. Kim, and K. Char, Appl. Phys. Lett. **102**, 252105 (2013).

[22]D. J. Singh, Q. Xu, and K. P. Ong, Appl. Phys. Lett. **104**, 011910 (2014).

[23]H.P.R Frederik and W. R. Hosler, Phys. Rev. **161**, 822 (1967).

[24]G. Herranz, M. Basletić, M. Bibes, C. Carrétéro, E. Tafra, E. Jacquet, K. Bouzehouane, C. Deranlot, A. Hamzić, J. M. Broto, A. Barthélémy, and A. Fert, Phys. Rev. Lett. **98**, 216803 (2007).

[25]X. Luo, Y. S. Oh, A. Sirenko, P. Gao, T. A. Tyson, K. Char, and S. W. Cheong, Appl. Phys. Lett. **100**, 172112 (2012).

[26]M. Mayer, AIP Conf. Proc. **475**, 541 (1999).

[27]See supplementary material at [URL will be inserted by AIP]for XRR fitting and AFM images.

[28]D. Seo, K. Yu, Y. J. Chang, E. Sonh, K.H. Kim, and E. J. Choi, Appl. Phys. Lett. **104**, 022102 (2014).

[29]F. D. Morrison, A. M. Coats, D. C. Sinclair, and A. R. West, J. Electroceram. **6**, 219 (2001).

[30]M. Vollman and R. Waser, J. Am. Ceram. Soc. **77**, 235 (1994).

[31]H. J. Kim, U. Kim, H. M. Kim, T. H. Kim, H. S. Mun, B. G. Jeon, K. T. Hong, W. J. Lee, C. Ju, K. H. Kim, and K. Char, Appl. Phys. Express **5**, 061102 (2012).

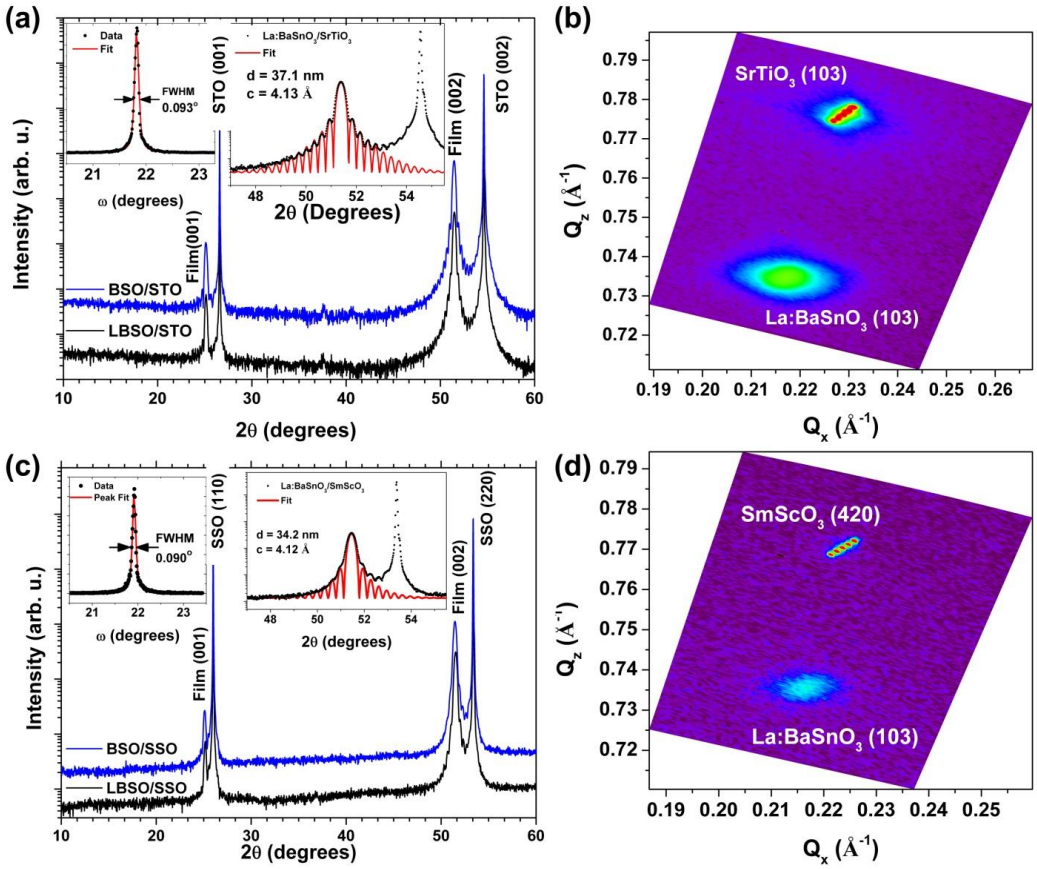

Figure 1(a) and (c):- θ-2θ scans for the BSO and LBSO films on STO and SSO substrates. Left inserts in (a) and (c) shows the rocking curve data with fitting of the full width half maximum, while the middle insert shows the Pendellosung fringes with the associated fitting to derive the thickness. (b) Reciprocal space maps around STO (103) reflection (d) Reciprocal space maps around SSO (420) reflection.

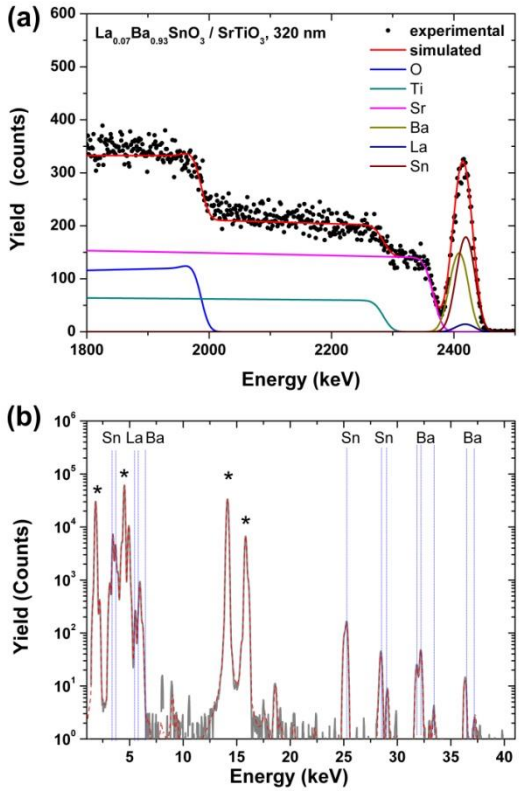

Figure 2 (a): Rutherford back scattering measurements for the thicker films along with the data fittings shown by red line. (b) PIXE spectra of the $La_{0.07}Ba_{0.93}SnO_3$ films on $SrTiO_3$ substrates. Dotted lines indicate emission from thin film elements. The asterisks (*) indicate emission from the substrate elements.

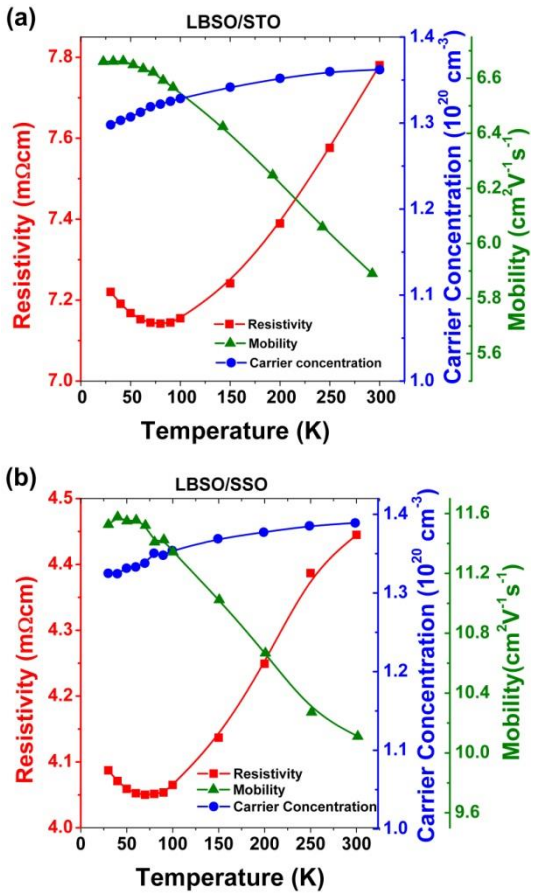

Figure 3(a) and (b):- Temperature dependent resistivity, mobility and carrier concentration measurements for LBSO films on STO and SSO substrates respectively.